

Diagnostic performance of total-body ^{18}F -FDG PET/CT with fast 2-min acquisition for liver tumours: Comparison with conventional PET/CT

Yan Hu

Department of nuclear medicine, Zhongshan Hospital, Fudan University

Guobing Liu

Department of nuclear medicine, Zhongshan hospital, Fudan university

Haojun Yu

Department of nuclear medicine, Zhongshan hospital, Fudan university

Jianying Gu

Department of plastic surgery, Zhongshan hospital, Fudan university

Hongcheng Shi (✉ shi.hongcheng@zs-hospital.sh.cn)

Department of nuclear medicine, zhongshan hospital, Fudan university

Research Article

Keywords: Total-body PET/CT, fast acquisition, diagnostic performance, liver tumours

Posted Date: November 17th, 2021

DOI: <https://doi.org/10.21203/rs.3.rs-1074707/v1>

License: © ⓘ This work is licensed under a Creative Commons Attribution 4.0 International License.

[Read Full License](#)

Version of Record: A version of this preprint was published at European Journal of Nuclear Medicine and Molecular Imaging on March 28th, 2022. See the published version at <https://doi.org/10.1007/s00259-022-05772-2>.

Abstract

Purpose

To comparatively evaluate the diagnostic performances of total-body ^{18}F -FDG PET/CT with fast 2-min acquisition and conventional PET/CT in liver cancer patients.

Methods This study included 156 patients with liver tumours. Seventy-eight patients underwent total-body PET/CT. PET raw data were reconstructed using acquisition durations of 2 min (G2) and 15 min (G15). Another 78 patients with liver lesions (control patients) underwent conventional uMI780 PET/CT (G780). All patients were evaluated based on TNM staging. The maximum tumour standardized uptake value (tumour SUVmax), mean normal liver SUV (SUVmean), and tumour SUVmax-to-liver SUVmean ratio (TLR) were determined for all patients. G15 data were used as the reference in the lesion detectability analysis. The diagnostic performances of PET/CT in terms of visual parameters and of PET in terms of semi-quantitative parameters such as SUVmax and TLR were evaluated. Receiver operating characteristics (ROC) curve analysis of SUVmax and TLR at G2 was performed. Pathologic findings of surgical specimens served as the gold standard for all patients.

Results The lesions found in G15 were also noted in G2; three lymph nodes were missed in G2; however, no significant difference was found in the TNM stage among G2, G15, and G780. For benign and malignant lesions, the liver SUVmean in G2 and G15 was higher than that in G780 (all $P < 0.05$). The tumour SUVmax and TLR in G2 were equivalent to those in G15 and G780 regardless of whether the lesions were benign or malignant. ROC curve analysis (SUVmax cut-off: 4.34, TLR cut-off: 1.34) demonstrated that G2 also had good sensitivity in detecting liver cancer.

Conclusion The diagnostic performance of total-body PET/CT in G2 was comparable to that in G15 among liver cancer patients. Further, the diagnostic efficiency of total-body PET/CT imaging with fast 2-min acquisition and conventional PET/CT was similar.

Introduction

Liver cancer is one of the most common and fatal cancers worldwide and the seventh leading cause of cancer death [1]. The incidence of liver cancer is higher in undeveloped countries, especially Asian countries [1–3]. In China, liver cancer is one of the five leading causes of years of death [4]. The prognosis of liver cancer is extremely poor. Moreover, surgical resection is feasible only in patients with early-stage liver cancer; therefore, accurate tumour staging is necessary in clinical settings [2, 5]. ^{18}F -FDG PET/CT may not be well-suited for well-differentiated hepatocellular carcinoma (HCC) due to its low sensitivity; however, it has a potential for application in the detection of poorly and moderately differentiated or advanced HCC [6, 7]. In recent years, great progress has been made in the use of ^{18}F -FDG PET/CT in the management of liver cancer, particularly in the staging of the disease [8, 9].

In PET/CT, image quality and noise level are mainly governed by the administered activity and acquisition time [10]. For conventional PET/CT, a short time acquisition duration per bed position can be achieved by a higher FDG activity. The minimum time-mass activity-product (TAP) is 7 or 14 MBq·min/kg for a PET system that applies a PET bed overlap of $\leq 30\%$ or $>30\%$ [11]. However, for the current state-of-the-art PET/CT, total-body PET/CT is performed with a 194-cm-long axial field of view (FOV) and a wide acceptance angle, allowing simultaneous recording of coincident photons from the whole body and greatly increasing PET scanner sensitivity [12]. Based on this physical characteristic, the TAP of ^{18}F -FDG can be further reduced and excellent image quality can be obtained with shortened scan durations or low injected activity in theory. Liu et al. have demonstrated the feasibility of the kinetics of ultra-low injected activity (10× reduction) and short-time acquisition (45 min) in healthy volunteers by using total-body PET/CT [13, 14]. However, ongoing studies have been mostly based on the evaluation of the image quality and are still in the preliminary stage of clinical feasibility [15, 16].

Total-body PET/CT enables the application of various combinations according to the injected activity and acquisition time to meet the different needs in clinical settings. The key to the value of PET/CT imaging is that the degree of lesion uptake is different from that in the background. However, the ^{18}F -FDG uptake capacity of different tissues or organs varies. For lesions with the same uptake of imaging agents, the visual detectability is likely to significantly differ if lesions are located in different organs. For example, the lesions in the rectum are obvious, while liver metastases or brain metastases of rectal cancer are less clearly visible due to ^{18}F -FDG hypermetabolism in the liver and brain and could be easily misdiagnosed. We established the acquisition time for different injected activities based on the overall image quality: 2 min was the shortest acquisition time that could be applied without compromising image quality and lesion detectability for the full activity. To provide a basis for appropriate application in clinical settings, we comparatively evaluated the diagnostic performance between total-body PET/CT and conventional PET/CT in liver cancer patients with the same injected activity and acquisition time of each bed in this study.

Materials And Methods

Patients

One hundred and fifty-six patients with liver tumours were retrospectively included, of which 78 patients with liver disease had undergone total-body PET/CT imaging from October 2019 to August 2020. The diagnosis of all patients was confirmed by postoperative pathological testing. The exclusion criteria were as follows: disease in the liver precluding measurement of mean normal liver standardised uptake value (SUV), a lack of pathological test results, and receipt of any treatment before PET/CT scanning. In a matched-pair study, another 78 patients who underwent conventional PET/CT imaging were selected from our dataset based on the characteristics and pathological test results of the patients who had undergone whole-body PET/CT scanning. This study was approved by the institutional review board of Zhongshan Hospital, Fudan University, and written informed consent was obtained.

PET/CT Image Acquisition and Reconstruction

All the patients fasted for at least 6 h before ^{18}F -FDG administration, and the level of fasting blood glucose was lower than 11 mmol/L. All of them were in an optimal hydration state and rested for approximately 60 min in quiet surroundings after ^{18}F -FDG injection. Seventy-eight patients underwent total-body PET/CT using the uEXPLORER scanner (United Imaging Healthcare, Shanghai, China). The PET images were acquired with 15 min and then reconstructed using the data for the first 2 min to simulate faster acquisition, hereinafter referred to as G15 and G2, respectively. PET reconstructions were performed using the ordered subset expectation maximization (OSEM) algorithm with the following parameters: time of flight (TOF) and point spread function (PSF) modelling, three iterations, and 20 subsets, slice thickness of 1.443 mm, matrix of 192×192 , and a full width at half maximum of the Gaussian filter function of 3 mm.

Another 78 patients (the control group) underwent conventional PET/CT (uMI780 scanner; United Imaging Healthcare, Shanghai, China) with a speed of 2 min/bed, which is referred to as G780. The PET image reconstruction algorithm used the OSEM protocol: 2 iterations, 20 subsets, TOF and PSF technologies, and a full width at half maximum of the Gaussian filter function of 3 mm. PET/CT scanning was performed from the skull base to the mid-thigh.

PET/CT Image Interpretation

The PET images were independently assessed by two nuclear medicine physicians. The G2 and G15 PET images were loaded into the viewer by using software (uWS-MI, R001, United Imaging Healthcare). ^{18}F -FDG uptake in the liver lesions equal to or lower than the liver SUVmean was referred to as negative and that higher than the liver SUVmean was referred to as positive. Malignant and benign lesions were diagnosed based on the rater's experience. TNM staging for liver cancer was according to the eighth edition of the American Joint Committee on Cancer (AJCC) staging manual [17, 18]. All lesions including tumours and lymph nodes on total-body PET/CT imaging were counted, and the G15 data served as the reference. A 2D circular region-of-interest (ROI) with a diameter of 2 cm was manually drawn on the homogeneous area of the right lobe of the liver. The ROI was carefully drawn far away from lesions and large blood vessels. The maximum SUV of a lesion (SUVmax) and the liver SUVmean were recorded. The SUVmax of the lesion was determined using the corresponding PET transverse slice with the maximum diameter on CT images for a comparison of the image datasets. The tumour-to-background ratio (TLR) was calculated by dividing the lesion SUVmax by the liver SUVmean. The values reported by each observer were averaged for intergroup comparison.

Statistical Analysis

Statistical analyses were performed using SPSS 20.0 (IBM Corp., Armonk, NY, USA), GraphPad Prism 6.0 (GraphPad Software Inc., San Diego, California, USA), and MedCalc 11.4 (MedCalc Software Bvba, Ostend, Belgium). Numeric parameters are presented as mean \pm standard deviation, and categorical variables are described as frequencies. A p -value of <0.05 indicated statistical significance. Independent

sample t-test and Mann-Whitney U test were used to compare differences between the 2-min group and routine time group. Differences in categorical variables between the two groups were evaluated using the Chi-square test. Receiver operating characteristics (ROC) curve analysis was performed to determine the sensitivity, specificity, and optimal cut-off values.

Results

Patient Demographics

A summary of the characteristics of the patients in the G2, G15, and G780 groups is shown in Table 1. Seventy-eight patients who underwent total-body PET/CT were included (55 men and 23 women, mean age 59.56 ± 12.74 years). Of these, 53 patients had solitary tumours and 25 had multiple tumours. Another 78 patients underwent conventional PET/CT (54 men and 24 women, mean age 58.81 ± 12.27 years). Among these patients, 57 had solitary tumours and 21 had multiple tumours. A significant difference in tumour size was found between the G2, G15, and G780 groups ($P < 0.05$). Intergroup differences in other characteristics were not significant (all $P > 0.05$).

Table 1
Demographics of patients who underwent total-body PET/CT and conventional PET/CT

Characteristic	G2/G15	G780	P-value
Age (year, range)	59.56±12.74 (21-85)	58.81±12.27 (20-81)	0.626
Sex			0.861
Male (%)	55 (70.5%)	54 (69.2%)	
Female (%)	23 (29.5%)	24 (30.8%)	
Tumours			0.482
Solitary (%)	53 (67.9%)	57 (73.1%)	
Multiple (%)	25 (32.1%)	21 (26.9%)	
Tumour size (cm, range)	5.24±3.66 (1.0-25.1)	7.02±4.57 (1.5-20.2)	0.009 [§]
Pathological types			1.000
HCC II-III (%)	36 (46.2%)	34 (43.6%)	
ICC II-III (%)	24 (30.8%)	26 (33.3%)	
HCC-ICC II-III (%)	5 (6.4%)	3 (3.8%)	
Inflammation (%)	2 (2.6%)	2 (2.6%)	
Haemangioma (%)	3 (3.8%)	3 (3.8%)	
EHE (%)	1 (1.3%)	1 (1.3%)	
HBilIN I (%)	1 (1.3%)	1 (1.3%)	
SNN (%)	2 (2.6%)	2 (2.6%)	
DN (%)	2 (2.6%)	3 (3.8%)	
FNH (%)	1 (1.3%)	2 (2.6%)	
Angiosarcoma (%)	1 (1.3%)	1 (1.3%)	
HBilIN I, Hepatobiliary intraepithelial neoplasia I; SNN, solitary necrotic nodule; DN, dysplastic nodule; EHE, epithelioid haemangioendothelioma; FNH, focal nodular hyperplasia			
[§] $P < 0.05$			

Lesion detectability and between G2 and G15 and TNM stages in the two groups

As shown in Table 2. A total of 87 tumours, large or small, were identified in G2 and G15, and no tumours were missed in G2. Fifty-nine lymph nodes were identified in G15, while 56 lymph nodes were identified in G2; three missed lymph nodes were located in the portal vena cava space, hepatogastric space, and

cardiophrenic angle. The location of distant metastasis was the kidney in both G2 and G15. No significant difference was found in lesion detectability between G2 and G15 ($P > 0.05$).

Table 2
Lesion detectability and TNM stage of liver cancer patients in the G2, G15, and G780 groups

	G2	G15	P-value (#)	G780	P-value (‡)
Lesion detection☒					
Tumours	87	87		/	
Lymph nodes	56	59	0.854	/	
TNM stage†					1.000
Tx	63 (95.45%)	63 (95.45%)		62 (96.87%)	
N Stage			1.000		0.600
N0	44 (84.62%)	43 (82.69%)		44 (83.02%)	
N1	10 (71.43%)	10 (71.43%)		7 (63.64%)	
M Stage					1.000
M0	65 (98.48%)	65 (98.48%)		63 (98.44%)	
M1	1 (1.52%)	1 (1.52%)		1 (1.56%)	
☒ Number of lesions					
† Number of patients					
# Comparison between the G2 and G15 groups					
‡ Comparison between the G2 and G780 groups					

Among the 87 patients with total-body PET/CT imaging data, liver cancer was confirmed by pathological examination in 66 patients, of which 14 showed lymph node metastasis. In G2 and G15, 63 liver cancer patients, with one patient showing distal metastasis, were diagnosed based on rater's subjective experience. Ten cases of lymph node metastasis were diagnosed in G2 and G15, while 44 and 43 cases without metastasis were diagnosed in G2 and G15, respectively. The patients with liver cancer in the G2 group showed the same TNM stage as those in the G15 group ($P > 0.05$).

Another 78 patients underwent conventional uMI780 PET/CT scanning, of which 64 were confirmed to show liver cancer by pathological examination and 11 showed lymph node metastasis. In the G780 group, 62 liver cancer patients, including one with distal metastasis, were diagnosed by the same raters' evaluations; of these, seven of showed lymph node metastasis and 44 did not show metastasis.

In comparisons involving G780, the TNM stage in cancer patients was not influenced by the rapid (2 min) acquisition in total-body PET/CT imaging (all $P > 0.05$).

Diagnostic performances of G2, G15, and G780 in the detection of liver cancer

The diagnostic performances of G2, G15, and G780 in the detection of liver cancer were shown in Table 3. Sixty-three cancer patients and nine cases with benign neoplasm were diagnosed in G2 and G15, which included three false-positive patients (one patient with hepatobiliary intraepithelial neoplasia I, HBilIN I; one patient with solitary necrotic nodule, SNN; one patient with dysplastic nodule, DN), and three false-negative patients (two patients with HCC, one patient with ICC). The diagnostic performances of G2 and G15 were as follows: sensitivity, 95.45%; specificity, 75.0%; PPV, 95.45%; NPV, 75%; and diagnostic accuracy, 92.31%.

Table 3
Diagnostic performance in the G2, G15, and G780 groups

	G2	G15	G780
TP/FP	63/3	63/3	62/5
TN/FN	9/3	9/3	9/2
Sensitivity (n)	95.45% (63/66)	95.45% (63/66)	96.88% (62/64)
Specificity (n)	75.00% (9/12)	75.00% (9/12)	64.29% (9/14)
Accuracy (n)	92.31% (72/78)	92.31% (72/78)	91.03% (71/78)
PPV (n)	95.45% (63/66)	95.45% (63/66)	92.54% (62/67)
NPV (n)	75% (9/12)	75% (9/12)	81.82% (9/11)
TP, True positive; FP, false positive; TN, true negative; FN, false negative; PPV, positive predictive value; NPV, negative predictive value			
† Number of patients			

Among the 78 patients who underwent assessments with the uMI780 PET/CT scanner, 62 and 9 patients were diagnosed as showing malignant lesions and benign tumors, respectively, which included five false-positive cases (one patient with inflammation, one patient with SNN, two patients with focal nodular hyperplasia, FNH; one patient with HBilIN I) and two false-negative cases (two patients with HCC) were detected. The diagnostic performance as follows: sensitivity, 96.88%; specificity, 64.29%; PPV, 92.54%; NPV, 81.82%; and diagnostic accuracy, 91.03%.

Quantitative analysis of benign and malignant lesions in G2, G15, and G780

The quantitative analysis of benign and malignant lesions is shown in Table 4. For both benign and malignant lesions, no significant differences were found between G2 and G15 in the tumour SUVmax,

liver SUVmean, and TLR. G780 showed a lower liver SUVmean than G2 and G15 for both benign or malignant lesions (all $P < 0.05$), but the tumour SUVmax and TLR in G2 and G15 were equivalent to that in G780 ($P > 0.05$). The tumour SUVmax and TLR of malignant lesions in G2 were higher than those in benign lesions, while no significant difference was shown between them (Figure 2). The ROC curve analysis (tumour SUVmax cut-off = 4.34, TLR cut-off = 1.34) of G2 showed that the tumour SUVmax yielded AUCs of 0.812 (95% CI 0.703-0.894) with sensitivity and specificity of 75.81% and 81.80% respectively, while the TLR exhibited AUCs of 0.861 (95% CI 0.760-0.931) with sensitivity and specificity of 88.71% and 81.82%, respectively (Figure 3). However, the diagnostic performance did not differ from the tumour SUVmax and the TLR (AUCs 0.812 and 0.861; $P = 0.218$).

Table 4

The quantitative PET parameters of benign and malignant tumours in the G2, G15, and G780 groups

PET parameters	Benign			Malignant		
	G2	G15	G780	G2	G15	G780
Tumour SUVmax (g/mL)	3.96±1.59†	3.61±1.59†	4.69±3.53†	9.87±8.25	9.78±8.46	8.55±6.29
Liver SUVmean (g/mL)	2.65±0.61⊠	2.57±0.57⊠	2.07±0.36	2.68±0.37⊠	2.56±0.35⊠	2.32±0.39
TLR	1.58±0.93†	1.50±0.93†	2.17±1.33†	3.75±3.24	3.91±3.53	3.72±2.68
SUVmax, Maximum standardized uptake value; SUVmean, mean standardized uptake value; TLR, tumour SUVmax/liver SUVmean						
⊠ Compared to the G780 group ($P < 0.05$)						
† Compared to malignant lesions ($P < 0.05$)						

Discussion

A short acquisition time is desirable in terms of patient comfort, especially for patients who cannot tolerate the regular acquisition time, such as paediatric patients and seriously ill patients. Furthermore, short acquisition times can reduce the possibility of patient movement and the artifacts caused by respiratory motion during the scanning process, which can lead to attenuation correction errors and registration errors as a result of mismatch between PET and CT images [19, 20]. The total-body PET/CT system with a long FOV and a wide range of detection angle shows 40-fold higher sensitivity than the current clinical PET/CT scanners. The high sensitivity provides an opportunity for total-body scans in a single breath-hold and even motion-frozen scans of the heart and the gastrointestinal tract [21, 22]. The quality of PET images obtained with subsecond reconstruction in human patients was superior to that obtained with conventional methods, indicating the substantial potential of motion-frozen imaging in respiratory and cardiovascular function research [22].

The potential of the short acquisition time in total-body PET/CT systems has been evaluated in several studies [16, 22–26]. The image quality and lesion detectability using total-body PET/CT with shorter acquisition times has been confirmed in our previous study, which demonstrated that full activity (4.4 MBq/kg) with a 2-min acquisition time still yielded preferable image quality [16]. Moreover, our previous study demonstrated that the image quality obtained with half injected activity (full activity, 3.7 MBq/kg) and a short acquisition time was comparable to that of conventional PET/CT [27]. According to our latest study, the fast PET protocol even reduced the acquisition time to 30–45 s, and the tumour background ratio (TBR) in total-body PET/CT with a 45-s acquisition time was equivalent to that in conventional PET/CT [25]. However, their study included participants who were cancer patients and their lesion TBR was relatively higher than that in benign lesions. In addition to staging of malignant tumours, differential diagnosis of benign and malignant tumours is also important in clinical practice, especially for the lesions with lower uptake. In comparison with the standard 2-min/bed acquisition, rapid acquisition (30–45 s) was suitable for cases with special circumstances, such as those involving lymphoma patients who needed multiple PET/CT scans for therapeutic response evaluation, but it was also associated with the risk of missing the lesions. Different kinds of tumours show different biological behaviours, and their ^{18}F -FDG uptake may differ accordingly. Image quality is the premise and the detection of lesions is the key in the evaluation of diagnostic performance. In order to guarantee image quality and lesion detectability, a 2-min acquisition period for total-body PET/CT was selected in our study. The previous studies offered references in methodology for clinical applications based on image segmentation. However, the clinical value of total-body PET/CT with rapid acquisition in tumour patients was still unknown. Therefore, our study selected the liver as the study object, which is challenging for displaying lesions, and focused on the assessment of the diagnostic performance of the total-body PET/CT imaging with fast 2-min acquisition.

Our results demonstrated that three cases of lower-uptake lymph nodes were missed in G2 (one in an ICC patient without lymph node metastasis, and two others in the HCC and ICC patients with multiple lymph node metastasis). Thus, total-body PET/CT has made significant progress in sensitivity in comparison with conventional PET/CT, but it still has some limitations. Some lesions were often misdiagnosed when the difference in FDG uptake between the lesion and the background was small. The lesion detectability in our study was still equivalent to that in G15 and not affected by the TNM stage in cancer patients. In all 66 cancer patients, the sensitivity, specificity, accuracy, positive predictive value and negative predictive value were the same in the G2 and G15 groups. In comparisons with the G780 group, the diagnostic performance was not compromised by shortening the acquisition time in total-body PET/CT.

For both benign or malignant lesions, the liver SUVmean in the G780 group was lower than those in the G2 and G15 groups. This trend was consistent with our previous study, which demonstrated that the liver SUVmean in the G2 group with half-low activity was higher than that in the full-activity group [15]. We hypothesized that the high liver SUVmean value was generated by the ultrasensitive characteristics of total-body PET/CT. Moreover, in total-body PET/CT, the patient posture involved placing the hands on the sides of the body, which could influence the attenuation correction of PET images. However, in

comparison with the G15 and G780 groups, the tumour SUVmax and TLR in the G2 group did not fluctuate too much due to the shortened acquisition time. Both of them yielded balanced sensitivity and specificity in the prediction of liver cancer. The fast 2-min acquisition still provided good diagnostic performance for liver cancer in total-body PET/CT imaging.

Our previous study showed that the image quality of total-body PET/CT with a 30–45 s acquisition time was equivalent to that of conventional PET/CT. The hypersensitivity of total-body PET/CT can yield better image quality and further improve the diagnostic efficiency. In comparison with the results for G15, several lesions were still missed in G2 in this study. This fully reflects the importance of obtaining sufficient effective counts for longer time acquisition to improve detective efficiency. However, the axial FOV of conventional PET/CT was limited, and long acquisition times are difficult to use in clinical practice since patient discomfort increases with extension of the acquisition time and patients are more likely to move in the process of scanning. Given the physical characteristics of total-body PET/CT, the image quality can be further improved by appropriately prolonging the acquisition time in a single bed. Thus, adjustment and adoption of personalized acquisition times by understanding the physiological characteristics of different organs and the uptake of ^{18}F -FDG and evaluation of the pathological characteristics of the disease according to the clinical information and inferring their uptake of imaging agents will have great significance in further improving the diagnostic performance and maintaining appropriate workflow in the clinic.

Our study had several limitations. First, the number of cases in this study was small, only 12 and 14 patients in the G2 and G780 groups had benign lesions confirmed by pathology, and the small number of benign cases contributed to the low specificity and negative predictive value. Second, the study did not strictly employ a head-to-head match: the demographic and pathological features were well-matched, but some marginal differences still remained. A proper head-to-head evaluation will be conducted in the future to eliminate this bias. Third, truncation artifacts on PET/CT images should be considered. The scanning posture in total-body PET/CT involved placing the hands on the sides of the body, while the posture in G780 involving raising the arms raised above the hands; the hard beam artifacts generated by this posture might interfere with the attenuation correction of PET images. Last, the 2D ROI was placed automatically at the same slice for the total-body PET images, which did not necessarily capture the true SUVmax of the whole tumour due to the limitations of the current measurement software.

In conclusion, fast 2-min acquisition with total-body PET/CT yielded equivalent diagnostic value as 15-min acquisition in total-body PET/CT and the conventional PET/CT imaging in liver cancer. The diagnostic performance of total-body PET/CT in liver cancer patients was not comprised by fast acquisition.

Declarations

Funding

This study is supported by the National Science Foundation for Scholars of China (Grant No. 81871407 to H.C.S.) and Shanghai Municipal Key Clinical Specialty (No. shslczdzk03401), Three-year Action Plan of Clinical Skills and Innovation of Shanghai Hospital Development Center (No. SHDC2020CR3079B to H.C.S.), the Shanghai Science and Technology Committee (No. 20DZ2201800), Three-year Action Plan for the fifth round of public health system construction in Shanghai (No. GWV-10.1-XK10). and Next Generation Information Infrastructure Construction Project (No. 201901014). No other potential conflicts of interest relevant to this article exist.

Conflicts of interest

The authors declare that they have no conflicts of interest.

Authors' Contributions

We acknowledge the contributions of all members involved in this article. Y.H. and H.C.S. contributed to the study design. Y.H. and G.B.L. contributed to the data processing and analysis. H.J.Y contributed to the image acquisition and processing. Y.H. and H.C.S. contributed to the manuscript drafting. J.Y.G and H.C.S. contributed to the article revising. All authors discussed and approved the final manuscript.

References

1. Bray F, Ferlay J, Soerjomataram I, Siegel RL, Torre LA, Jemal A. Global cancer statistics 2018: GLOBOCAN estimates of incidence and mortality worldwide for 36 cancers in 185 countries. *CA Cancer J Clin*. 2018;68(6):394–424. 10.3322/caac.21492.
2. Anwanwan D, Singh SK, Singh S, Saikam V, Singh R. Challenges in liver cancer and possible treatment approaches. *Biochimica Biophysica Acta Rev Cancer*. 2020;1873(1):188314. 10.1016/j.bbcan.2019.188314.
3. Starley BQ, Calcagno CJ, Harrison SA. Nonalcoholic fatty liver disease and hepatocellular carcinoma: A weighty connection. *Hepatology*. 2010;51(5):1820–1832. 10.1002/hep.23594.
4. Zhou M, Wang H, Zeng X, Yin P, Zhu J, Chen W, et al. Mortality, morbidity, and risk factors in China and its provinces, 1990–2017: a systematic analysis for the Global Burden of Disease Study 2017. *The Lancet*. 2019;394(10204):1145–1158. 10.1016/S0140-6736(19)30427-1.
5. Benson AB, D'Angelica MI, Abbott DE, Abrams TA, Alberts SR, Anaya DA, et al. Guidelines Insights: Hepatobiliary Cancers, Version 2.2019. *J Natl Compr Canc Netw*. 2019;17(4):302–310. 10.6004/jnccn.2019.0019.
6. Ayuso C, Rimola J, Vilana R, Burrel M, Darnell A, Garcia-Criado A, et al. Diagnosis and staging of hepatocellular carcinoma (HCC): current guidelines. *Eur J Radiol*. 2018;101:72–81. 10.1016/j.ejrad.2018.01.025.
7. Na SJ, Oh JK, Hyun SH, Lee JW, Hong IK, Song B, et al. 18F-FDG PET/CT Can Predict Survival of Advanced Hepatocellular Carcinoma Patients: A Multicenter Retrospective Cohort Study. *J Nucl Med*.

- 2017;58(5):730–736. 10.2967/jnumed.116.182022.
8. Lee SM, Kim HS, Lee S, Lee JW. Emerging role of (18)F-fluorodeoxyglucose positron emission tomography for guiding management of hepatocellular carcinoma. *World J Gastroenterol*. 2019;25(11):1289–1306. 10.3748/wjg.v25.i11.1289.
 9. Lu R, She B, Gao W, Ji Y, Xu D, Wang Q, et al. Positron-emission tomography for hepatocellular carcinoma: Current status and future prospects. *World J Gastroenterol*. 2019;25(32):4682–4695. 10.3748/wjg.v25.i32.4682.
 10. Schiller F, Frings L, Thurow J, Meyer PT, Mix M. Limits for Reduction of Acquisition Time and Administered Activity in (18)F-FDG PET Studies of Alzheimer Dementia and Frontotemporal Dementia. *J Nucl Med*. 2019;60(12):1764–1770. 10.2967/jnumed.119.227132.
 11. Boellaard R, Delgado-Bolton R, Oyen WJG, Giammarile F, Tatsch K, Eschner W, et al. FDG PET/CT: EANM procedure guidelines for tumour imaging: version 2.0. *Eur J Nucl Med Mol I*. 2015;42(2):328–354. 10.1007/s00259-014-2961-x.
 12. Spencer BA, Berg E, Schmall JP, Omidvari N, Leung EK, Abdelhafez YG, et al. Performance Evaluation of the uEXPLORER Total-Body PET/CT Scanner Based on NEMA NU 2-2018 with Additional Tests to Characterize PET Scanners with a Long Axial Field of View. *J Nucl Med*. 2021;62(6):861–870. 10.2967/jnumed.120.250597.
 13. Liu G, Hu P, Yu H, Tan H, Zhang Y, Yin H, et al. Ultra-low-activity total-body dynamic PET imaging allows equal performance to full-activity PET imaging for investigating kinetic metrics of 18F-FDG in healthy volunteers. *Eur J Nucl Med Mol I*. 2021. 10.1007/s00259-020-05173-3.
 14. Liu G, Yu H, Shi D, Hu P, Hu Y, Tan H, et al. Short-time total-body dynamic PET imaging performance in quantifying the kinetic metrics of (18)F-FDG in healthy volunteers. *Eur J Nucl Med Mol I*. 2021. 10.1007/s00259-021-05500-2.
 15. Tan H, Sui X, Yin H, Yu H, Gu Y, Chen S, et al. Total-body PET/CT using half-dose FDG and compared with conventional PET/CT using full-dose FDG in lung cancer. *Eur J Nucl Med Mol I*. 2021;48(6):1966–1975. 10.1007/s00259-020-05091-4.
 16. Zhang Y, Hu P, Wu R, Gu Y, Chen S, Yu H, et al. The image quality, lesion detectability, and acquisition time of 18F-FDG total-body PET/CT in oncological patients. *Eur J Nucl Med Mol I*. 2020;47(11):2507–2515. 10.1007/s00259-020-04823-w.
 17. Lamarca A, Santos Laso A, Utpatel K, La Casta A, Stock S, Forner A, et al. Liver Metastases of Intrahepatic Cholangiocarcinoma: Implications for an Updated Staging System. *Hepatology (Baltimore, Md.)*. 2021;73(6):2311–2325. 10.1002/hep.31598.
 18. Amin MB, Greene FL, Edge SB, Compton CC, Gershenwald JE, Brookland RK, et al. The Eighth Edition AJCC Cancer Staging Manual: Continuing to build a bridge from a population-based to a more "personalized" approach to cancer staging. *CA Cancer J Clin*. 2017;67(2):93–99. 10.3322/caac.21388.
 19. Liu C, Pierce li LA, Alessio AM, Kinahan PE. The impact of respiratory motion on tumor quantification and delineation in static PET/CT imaging. *Phys Med Biol*. 2009;54(24):7345–7362. 10.1088/0031-

20. Nehmeh SA, Erdi YE. Respiratory motion in positron emission tomography/computed tomography: a review. *Semin Nucl Med.* 2008;38(3):167–76. 10.1053/j.semnuclmed.2008.01.002.
21. Zhang X, Zhou J, Cherry SR, Badawi RD, Qi J. Quantitative image reconstruction for total-body PET imaging using the 2-meter long EXPLORER scanner. *Phys Med Biol.* 2017;62(6):2465–2485. 10.1088/1361-6560/aa5e46.
22. Zhang X, Cherry SR, Xie Z, Shi H, Badawi RD, Qi J. Subsecond total-body imaging using ultrasensitive positron emission tomography. *Proceedings of the National Academy of Sciences - PNAS.* 2020;117(5):2265-2267. 10.1073/pnas.1917379117.
23. Badawi RD, Shi H, Hu P, Chen S, Xu T, Price PM, et al. First Human Imaging Studies with the EXPLORER Total-Body PET Scanner. *J Nucl Med.* 2019;60(3):299–303. 10.2967/jnumed.119.226498.
24. Pantel AR, Viswanath V, Daube-Witherspoon ME, Dubroff JG, Muehllehner G, Parma MJ, et al. PennPET Explorer: Human Imaging on a Whole-Body Imager. *J Nucl Med.* 2020;61(1):144–151. 10.2967/jnumed.119.231845.
25. Hu P, Zhang Y, Yu H, Chen S, Tan H, Qi C, et al. Total-body (18)F-FDG PET/CT scan in oncology patients: how fast could it be? *Eur J Nucl Med Mol I.* 2021;48(8):2384–2394. 10.1007/s00259-021-05357-5.
26. Xiao J, Yu H, Sui X, Hu Y, Cao Y, Liu G, et al. Can the BMI-based dose regimen be used to reduce injection activity and to obtain a constant image quality in oncological patients by (18)F-FDG total-body PET/CT imaging? *Eur J Nucl Med Mol I.* 2021. 10.1007/s00259-021-05462-5.
27. Tan H, Sui X, Yin H, Yu H, Gu Y, Chen S, et al. Total-body PET/CT using half-dose FDG and compared with conventional PET/CT using full-dose FDG in lung cancer. *Eur J Nucl Med Mol I.* 2020;2020 Nov 27. 10.1007/s00259-020-05091-4.

Figures

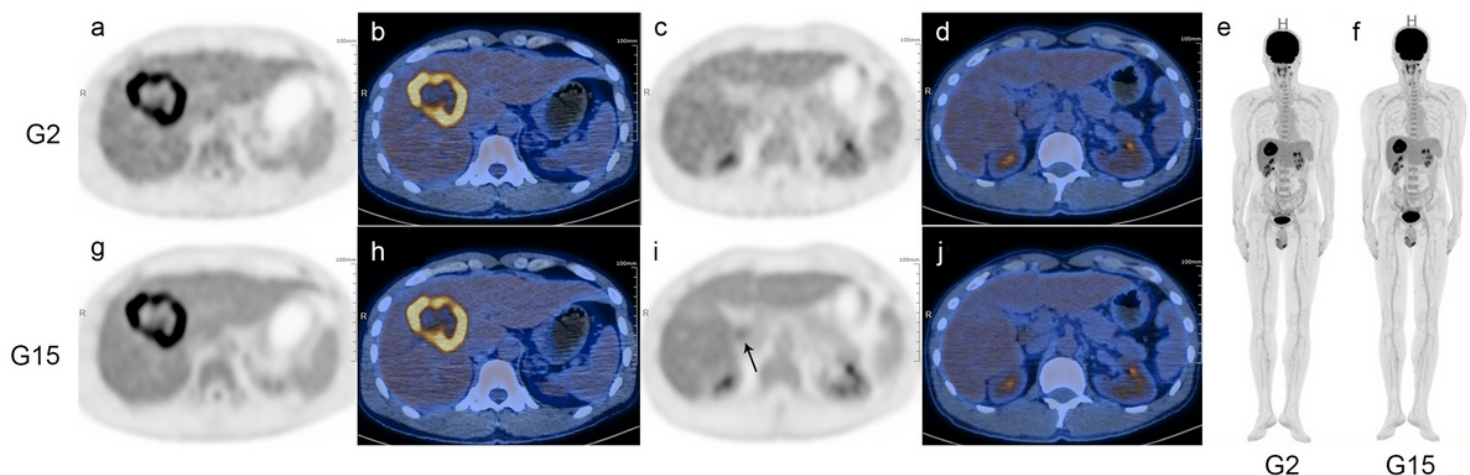


Figure 1

PET images of a 39-year-old patient with ICC Transverse views of the intense uptake of lesions in the liver (a-PET, b-Mixed) and the lymph node (c-PET, d-Mixed) and a coronal slice of the whole body (e) in G2. Transverse views of the intense uptake of lesions in the liver (g-PET, h-Mixed) and the lymph node (i-PET, j-Mixed) and a coronal slice of the whole body (f) in G15. The lymph node shown in G15 was missed in G2 (c, l-arrow).

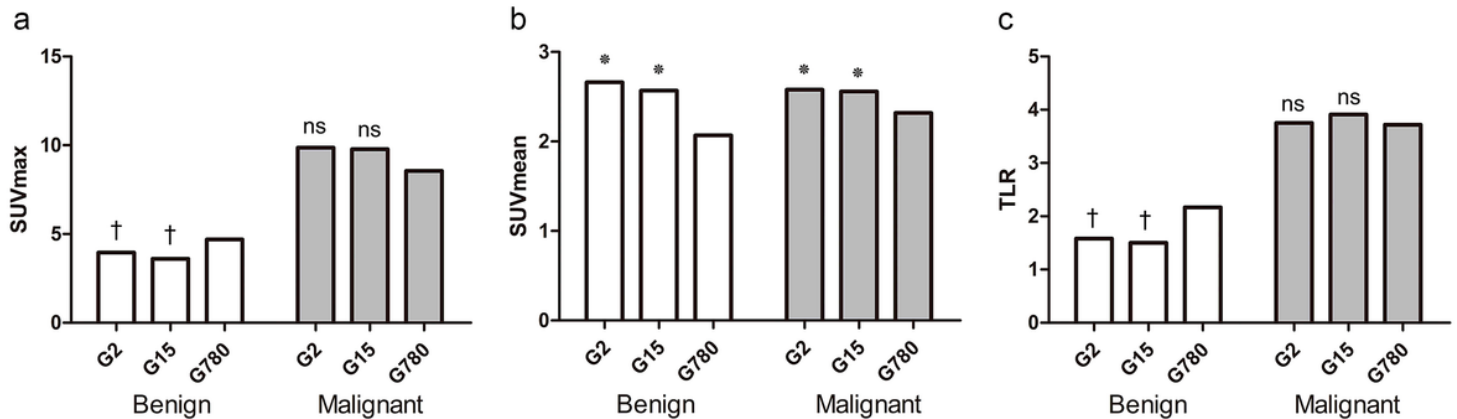


Figure 2

The box blot of tumour SUVmax, liver SUVmean and TLR of benign and malignant tumours in G2, G15, and G780 (a-c). The liver SUVmean of the G2 and G15 groups was higher than that in the G780 group in benign and malignant lesions, while the tumour SUVmax and TLR were equivalent to those in the G780 group. The SUVmax and TLR in malignant lesions were higher than those in benign lesions ($P < 0.05$). * Compared with G780 ($P < 0.05$). † Compared with malignant lesions ($P < 0.05$)

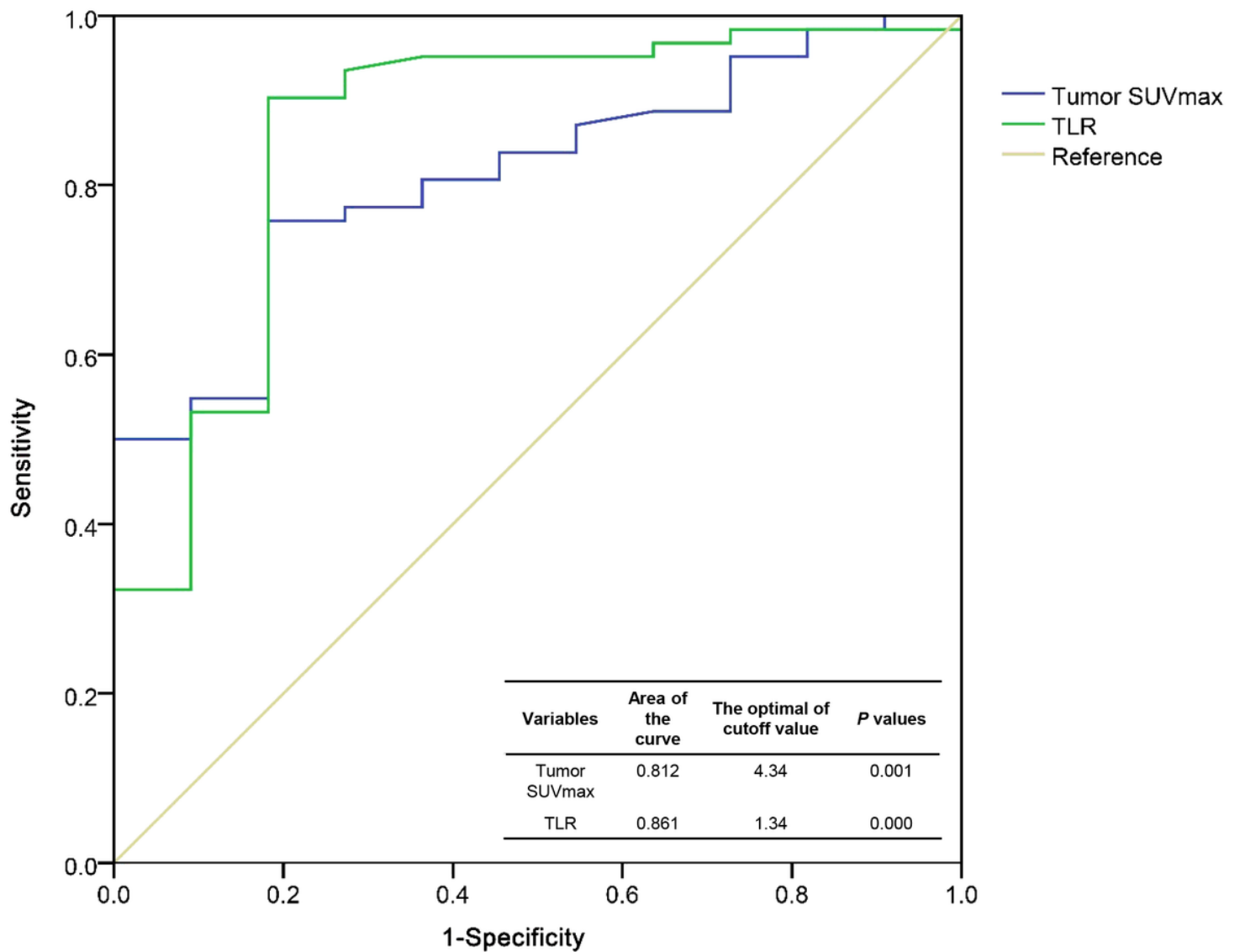


Figure 3

The receiver operating characteristic curves (ROC) for tumour SUVmax and TLR in prediction of malignant lesions in G2. The area under the curve (AUC) for tumour SUVmax and TLR were 0.812 and 0.861. The sensitivity of both indicators was 75.81% and 88.71%, and specificity was 81.80% and 81.82%. The diagnostic performance of the tumour SUVmax and TLR showed no significant difference.